Glyoxal yield from isoprene oxidation and relation to formaldehyde: chemical mechanism, constraints from SENEX aircraft observations, and interpretation of OMI satellite data

Christopher Chan Miller[1], Daniel J. Jacob[1,2], Eloise A. Marais[1], Karen Yu[2], Katherine R. Travis[2], Patrick S. Kim[1], Jenny A. Fisher[3], Lei Zhu[2], Glenn M. Wolfe[4,5], Thomas F. Hanisco[4], Frank N. Keutsch[2,6], Jennifer Kaiser[7,a], Kyung-Eun Min[8,9,b], Steven S. Brown[9,10], Rebecca A. Washenfelder[8,9], Gonzalo González Abad[11], and Kelly Chance[11]

[1]Department of Earth and Planetary Sciences, Harvard University, Cambridge, MA, USA
[2]School of Engineering and Applied Sciences, Harvard University, Cambridge, MA, USA
[3]School of Chemistry and School of Earth and Environmental Sciences, University of Wollongong, Wollongong, NSW, Australia
[4]Atmospheric Chemistry and Dynamics Lab, NASA Goddard Space Flight Center, Greenbelt, MD, USA
[5]Joint Center for Earth Systems Technology, University of Maryland Baltimore County, Baltimore, MD, USA
[6]Department of Chemistry and Chemical Biology, Harvard University, Cambridge, MA, USA
[7]Department of Chemistry, University of Wisconsin Madison, Madison, WI, USA
[8]Cooperative Institute for Research in Environmental Sciences, University of Colorado Boulder, Boulder, CO, USA
[9]Chemical Sciences Division, NOAA Earth System Research Laboratory, Boulder, CO, USA
[10]Department of Chemistry and Biochemistry, University of Colorado, Boulder, CO, USA
[11]Harvard-Smithsonian Center for Astrophysics, Cambridge MA, USA
[a]now at: School of Engineering and Applied Sciences, Harvard University, Cambridge MA, USA
[b]now at: School of Earth Sciences and Environmental Engineering, Gwangju Institute of Science and Technology, Gwangju, South Korea

Correspondence to: Daniel Jacob (djacob@fas.harvard.edu)

Abstract.

Glyoxal (CHOCHO) is produced in the atmosphere by the oxidation of volatile organic compounds (VOCs). Like formaldehyde (HCHO), another VOC oxidation product, it is measurable from space by solar backscatter. Isoprene emitted by vegetation is the dominant source of CHOCHO and HCHO in most of the world. We use aircraft observations of CHOCHO and HCHO from the SENEX campaign over the Southeast US in Summer 2013 to better understand the CHOCHO time-dependent yield from isoprene oxidation, its dependence on nitrogen oxides ($NO_x \equiv NO + NO_2$), the behaviour of the CHOCHO-HCHO relationship, the quality of OMI CHOCHO satellite observations, and the implications for using CHOCHO observations from space as constraints on isoprene emission. We simulate the SENEX and OMI observations with the GEOS-Chem chemical transport model featuring a new chemical mechanism for CHOCHO formation from isoprene. The mechanism includes prompt CHOCHO formation under low-NO_x conditions following the isomerization of the isoprene peroxy radical ($ISOPO_2$). The SENEX observations provide support for this prompt CHOCHO formation pathway, and are generally consistent with the GEOS-Chem mechanism. Boundary layer CHOCHO and HCHO are strongly correlated in the observations and the model, with some departure under low-NO_x conditions due to prompt CHOCHO formation. SENEX vertical profiles indicate a free tropospheric

CHOCHO background that is absent from the model. The OMI CHOCHO data provide some support for this free tropospheric background and show Southeast US enhancements consistent with the isoprene source but a factor of 2 too low. Part of this OMI bias is due to excessive surface reflectivities assumed in the retrieval. The OMI CHOCHO and HCHO seasonal data over the Southeast US are tightly correlated and provide redundant proxies of isoprene emission. Higher temporal resolution in future geostationary satellite observations may enable detection of the prompt CHOCHO production under low-NO_x conditions apparent in the SENEX data.

1 Introduction

Glyoxal (CHOCHO) and formaldehyde (HCHO) are short-lived products of the atmospheric oxidation of volatile organic compounds (VOCs). Both are detectable from space by solar backscatter (Chance et al., 2000; Wittrock et al., 2006). Isoprene emitted by terrestrial vegetation accounts for about a third of the global source of non-methane VOCs (NMVOCs) (Guenther et al., 2012) and drives large enhancements of CHOCHO and HCHO in the continental boundary layer (Palmer et al., 2003; Fu et al., 2008). Satellite observations of HCHO have been widely used as a proxy to estimate isoprene emission (Abbot et al., 2003; Palmer et al., 2006; Millet et al., 2008; Curci et al., 2010; Barkley et al., 2013), but there are uncertainties related to the HCHO yield from isoprene oxidation (Marais et al., 2012) and the role of other NMVOCs as HCHO precursors (Fu et al., 2007). CHOCHO observations from space could provide a complementary constraint (Vrekoussis et al., 2009, 2010; Alvarado et al., 2014; Chan Miller et al., 2014). Here we use CHOCHO and HCHO aircraft observations over the Southeast United States from the Summer 2013 Southeast Nexus (SENEX) campaign (Warneke et al., 2016), interpreted with the GEOS-Chem chemical transport model (CTM), to test understanding of the CHOCHO yield from isoprene oxidation, its dependence on nitrogen oxide radicals ($NO_x \equiv NO + NO_2$), and the combined value of the HCHO-CHOCHO pair measured from space to constrain isoprene emissions and chemistry.

Isoprene impacts air quality and climate as a precursor to ozone (Geng et al., 2011) and secondary organic aerosol (SOA) (Carlton et al., 2009), and also affects concentrations of hydrogen oxide radicals ($HO_x \equiv OH + HO_2$) (Peeters and Muller, 2010) and NO_x (Mao et al., 2013; Fisher et al., 2016). Atmospheric oxidation of isoprene by OH takes place on a timescale of less than an hour to produce organic peroxy radicals ($ISOPO_2$). Reaction of $ISOPO_2$ with NO drives production of ozone and of organic nitrates that serve as a reservoir for NO_x (Browne and Cohen, 2012). At lower NO_x levels, $ISOPO_2$ reacts dominantly with HO_2 to produce isoprene epoxydiols (IEPOX) via isoprene peroxides (ISOPOOH) (Paulot et al., 2009b), and from there isoprene SOA (Marais et al., 2016). $ISOPO_2$ can also isomerize to generate HO_x radicals (Peeters et al., 2009; Crounse et al., 2011; Peeters et al., 2014).

The fate of $ISOPO_2$ determines the production rates and overall yields of CHOCHO and HCHO. Several studies have provided insight on the time- and NO_x-dependent yield of HCHO (Palmer et al., 2003; Marais et al., 2012; Wolfe et al., 2016). Under high-NO_x conditions, HCHO production is sufficiently prompt that observed HCHO columns can be locally related to isoprene emission rates (Palmer et al., 2006). This assumption is the basis of many studies that have used satellite HCHO observations to constrain isoprene emissions (Palmer et al., 2006; Fu et al., 2007; Millet et al., 2008; Curci et al., 2010). HCHO

production is much slower under low-NO_x conditions, spatially "smearing" the local relationship between isoprene emissions and HCHO columns. This has been addressed by using concurrent satellite data for NO_2 columns to correct the isoprene-HCHO relationship (Marais et al., 2012) or by using adjoint-based inverse modeling to relate HCHO columns to isoprene emissions including the effect of transport (Fortems-Cheiney et al., 2012).

Isoprene is estimated to account for about $\sim 50\%$ of global CHOCHO production (Fu et al., 2008), but there is large uncertainty regarding the yield of CHOCHO from isoprene oxidation. Open fires and aromatic VOCs can also be major sources of CHOCHO (Volkamer et al., 2001; Fu et al., 2008; Chan Miller et al., 2016). Several studies have used the measured CHOCHO-HCHO concentration ratio $R_{GF} = [\mathrm{CHOCHO}]/[\mathrm{HCHO}]$ as an indicator of the dominant VOC precursors. Vrekoussis et al. (2010) found higher R_{GF} values (> 0.04) from GOME-2 satellite observations in regions where biogenic VOCs are dominant, and lower values where anthropogenic VOCs are dominant. However, the opposite behaviour is observed from ground-based studies (DiGangi et al., 2012). Our recent CHOCHO retrieval from the OMI satellite instrument (Chan Miller et al., 2014) is in better agreement with surface observations of CHOCHO and R_{GF} (Kaiser et al., 2015) compared to those from GOME-2 (Vrekoussis et al., 2010) and SCIAMACHY (Wittrock et al., 2006) as a result of improved background corrections and removal of NO_2 interferences. There remains the question of how observed CHOCHO-HCHO relationships are to be interpreted.

The Southeast Nexus (SENEX) aircraft campaign was conducted over the Southeast United States in June-July 2013. The aircraft had a detailed chemical payload including in situ CHOCHO (Min et al., 2016) and HCHO (Cazorla et al., 2015). Thirteen daytime flights were conducted over the campaign with extensive boundary layer coverage. (Li et al., 2016) recently used the SENEX observations to evaluate CHOCHO formation from isoprene in the AM3 CTM. They found that the AM3 mechanism had closer agreement with observations than the explicit Master Chemical Mechanism v3.3.1 (MCMv3.3.1) (Jenkin et al., 2015), and suggested that CHOCHO yields from isoprene epoxydiols are underestimated in MCMv3.3.1. Here we take a more rigorous look at potential missing pathways in MCMv3.3.1. In doing so, we present an improved chemical mechanism for CHOCHO formation from isoprene for the GEOS-Chem CTM, and evaluate it against the SENEX observations, including the time- and NO_x-dependence of the CHOCHO yield from isoprene. We discuss the implications of the new mechanism for the interpretation of satellite observations, and present a first validation of the CHOCHO retrieval from the OMI satellite instrument (Chan Miller et al., 2014).

2 GEOS-Chem Model Description

2.1 General Description

We use the same version of GEOS-Chem v9.2 (http://www.geos-chem.org) that has been used previously to interpret chemical observations from the NASA SEAC^{4}RS aircraft campaign conducted in the same Southeast US region in August-September 2013 (Travis et al., 2016; Fisher et al., 2016). The model is driven by assimilated meteorological data with $0.25^\circ \times 0.3125^\circ$ horizontal resolution from the Goddard Earth Observing System (GEOS-FP) reanalysis product (Molod et al., 2012). The native $0.25^\circ \times 0.3125^\circ$ resolution is retained in GEOS-Chem over the North American domain ($130^\circ - 60^\circ$W, $9.75^\circ - 60^\circ$N), nested within a global simulation at $2^\circ \times 2.5^\circ$ resolution (Kim et al., 2015). Isoprene chemistry in GEOS-Chem v9.2 is as described

by Mao et al. (2013), but the SEAC^{4}RS simulation includes a number of updates described by Travis et al. (2016) and Fisher et al. (2016). The simulation presented here includes further modifications relevant to CHOCHO, listed in the supplementary material (Table S1), and summarized below. Evaluation of the model with SEAC^{4}RS observations has been presented by Kim et al. (2015) for aerosols, Travis et al. (2016) for ozone and NO_x, Fisher et al. (2016) for organic nitrates, Marais et al. (2016) for isoprene SOA, and Zhu et al. (2016) for HCHO including satellite validation.

Isoprene emissions in the model are from MEGANv2.1 (Guenther et al., 2012) with a 15% reduction (Kim et al., 2015), and NO_x emissions are as described by Travis et al. (2016) including a 50% decrease in the anthropogenic source relative to the 2011 National Emission Inventory of the U.S. Environmental Protection Agency. Yu et al. (2016) pointed out that isoprene and NO_x emissions in the Southeast US are spatially segregated and show that the $0.25^\circ \times 0.3125^\circ$ resolution of GEOS-Chem is adequate for separating the populations of high- and low-NO_x conditions for isoprene oxidation.

2.2 CHOCHO formation from isoprene and loss

Figure 1 shows the CHOCHO formation pathways from isoprene oxidation by OH (the main isoprene sink) as implemented in this work. Oxidation is initiated by OH addition to the terminal carbons of the isoprene double bonds (positions 1 and 4, Figure 1). Isoprene peroxy radicals ($ISOPO_2$) are formed by O_2 addition to the carbon either in β or δ to the hydroxyl carbon. $ISOPO_2$ reacts with NO and HO_2, and also isomerizes. Together these pathways represent 92% of $ISOPO_2$ loss, with the remainder due to reactions with organic peroxy radicals.

Under high-NO_x conditions, CHOCHO is produced promptly via products of the δ isomers (HC5, DIBOO) (Paulot et al., 2009a; Galloway et al., 2011). CHOCHO production via the β isomers is slower, due to the intermediary production of methylvinylketone (MVK) followed by glycolaldehyde (GLYC). GEOS-Chem originally had a fixed δ vs. β branching ratio of 24% for the reaction of $ISOPO_2 + NO$, based on the chamber experiments of Paulot et al. (2009a). However recent work has shown that O_2 addition to the isoprene-OH adducts is reversible (pink pathway, Figure 1), allowing interconversion between β and δ $ISOPO_2$ isomers (Peeters et al., 2009; Crounse et al., 2011; Peeters et al., 2014). β isomers are heavily favoured at equilibrium, accounting for $\sim 95\%$ of $ISOPO_2$ (Peeters et al., 2014). The experimental conditions in Paulot et al. (2009a) used high NO concentrations (~ 500 ppbv). This implies short $ISOPO_2$ lifetimes, and thus may not reflect the degree of isomer interconversion seen at ambient oxidant levels. Here we adopt a $\delta - ISOPO_2$ branching ratio of 10%, following Fisher et al. (2016), to match SEAC^{4}RS observations of organic nitrates produced through the $\delta - ISOPO_2 + NO$ pathway.

CHOCHO forms under low-NO_x conditions through isoprene epoxydiols (IEPOX) and through the $ISOPO_2$ isomerization pathway. IEPOX forms as a second-generation non-radical product of isoprene oxidation via $ISOPOOH$, and thus represents a slow CHOCHO formation pathway. IEPOX isomer fractions in GEOS-Chem are based on equilibrium δ/β $ISOPO_2$ branching ratios (Bates et al., 2014; Travis et al., 2016). At low NO_x levels the $ISOPO_2$ lifetime is sufficiently long for equilibrium to be reached (Peeters et al., 2014). $ISOPO_2$ isomerization in the previous GEOS-Chem mechanism of Travis et al. (2016) produced solely hydroperoxyaldehydes (HPALDs), but here we also include the formation of dihydroperoxy α-formyl peroxy radicals (di-HPCARPs) (Peeters et al., 2014) following MCMv3.3.1. di-HPCARPs in MCMv3.3.1 have a low CHOCHO yield, but here we introduce a (1,5)H-shift isomerization of di-HPCARPs that could be competitive with the (1,4)H-shift isomerization due

to the presence of the terminal-peroxide functional group (Crounse et al., 2013). The resulting di-hydroperoxide dicarbonyl compound (DHDC) product quickly photolyzes to produce CHOCHO, analagous to the mechanisms proposed for HPALDs (Peeters et al., 2014) and carbonyl nitrates (Müller et al., 2014). As shown below, we find that this pathway can explain SENEX observations of prompt CHOCHO production under low-NO_x conditions.

The mechanism presented here differs substantially from the AM3 mechanism previously used by Li et al. (2016) to analyze the SENEX observations. Li et al. (2016) tested branching ratios of 22% and 0% for $\delta-ISOPO_2 + NO$, with the latter intended to reflect $ISOPO_2$ isomer interconversion. The 10% branching ratio in this study is constrained by SEAC^{4}RS organic nitrate observations (Fisher et al., 2016). Li et al. (2016) report a CHOCHO yield from GLYC oxidation (Section S1), which is mainly due to a lower CHOCHO yield from $GLYC + OH$ (13% vs. 20%). Their yield of CHOCHO from IEPOX is 28%, much higher than can be accommodated by yields of hydroxyacetone derived from IEPOX oxidation chamber experiments (Bates et al., 2014) (the expected coproduct of CHOCHO via this pathway, Section S2). Following Travis et al. (2016), we set the CHOCHO yield from IEPOX to the corresponding hydroxyacetone yields reported by Bates et al. (2014) (8.5% via HO_2 and 8.8% via NO). Finally AM3 assumes 25% CHOCHO yield from HPALD photolysis following Stavrakou et al. (2010), which has been used in many past studies (Mao et al., 2013; Marais et al., 2016). However HPALD photolysis is not expected to yield CHOCHO (Section S3). The CHOCHO formation pathway via DHDC proposed here can be justified from existing literature (Section S3). Inclusion of DHDC increases the yield of CHOCHO via $ISOPO_2$ isomerization by 18%, which is comparable to the AM3 yield.

Li et al. (2016) found that CHOCHO concentrations are sensitive to aerosol reactive uptake. Our standard model simulation does not include this uptake, but we conducted a sensitivity simulation with a reactive uptake coefficient $\gamma = 2 \times 10^{-3}$ from Li et al. (2016). We find that CHOCHO concentrations decrease by only 10% on average (Section S4) because competing CHOCHO sinks from reaction with OH and photolysis are fast.

2.3 Time- and NO_x-dependent CHOCHO and HCHO yields from isoprene

Understanding the time- and NO_x-dependent yields of CHOCHO and HCHO from isoprene oxidation is critical for interpreting observed CHOCHO and HCHO columns from space in terms of isoprene emissions. Here we examine time-dependent CHOCHO and HCHO molar yields in the GEOS-Chem and MCMv3.3.1 chemical mechanisms using the Dynamically Simple Model of Atmospheric Chemical Complexity (DSMACC) box model (Emmerson and Evans, 2009). Simulations are initiated at 9am local time with 1 ppbv isoprene, 40 ppbv O_3, and 100 ppbv CO. NO_x concentrations are held at fixed values. Photolysis rates are calculated for clear-sky with the TUV radiative transfer model (Madronich, 1987). To correct for differences in time-dependent yields associated with differences in OH concentrations, we reference GEOS-Chem and MCMv3.3.1 results to a common "OH exposure time" variable (t_{OH});

$$t_{OH} = \frac{1}{[OH]_{ref}} \int_0^t [OH](t')dt' \quad (1)$$

Here $[OH](t)$ is the OH concentration simulated in the box model, and $[OH]_{ref} = 4 \times 10^6$ molecules cm^{-3} is a reference OH concentration representative of summer daytime conditions over the Southeast US (Wolfe et al., 2016). For a fixed [OH]$= 4 \times 10^6$ molecules cm^{-3}, t_{OH} represents the actual time.

Figure 2 shows the time- and NO_x-dependent cumulative molar yields of CHOCHO and HCHO in GEOS-Chem and MCMv3.3.1. The branching ratio of $ISOPO_2$ as a function of NO_x is also shown. The time-dependent HCHO yields in both mechanisms are similar under high-NO_x conditions. Additional confidence in the HCHO yield under these conditions is offered by the ability of GEOS-Chem to reproduce the observed correlation between HCHO and isoprene organic nitrates (Mao et al., 2013; Fisher et al., 2016). The HCHO yield is lower under low-NO_x conditions in both mechanisms, and overall the difference between them is minor.

There is far more disagreement between the two mechanisms for CHOCHO yields. Under high-NO_x conditions, GEOS-Chem produces CHOCHO rapidly in the first two hours due to its higher $\delta-ISOPO_2 + NO$ branching ratio (10% in GEOS-Chem vs. 3.4% in MCMv3.3.1). This is compensated at longer OH-exposure times by higher GLYC yields from isoprene in MCMv3.3.1. GEOS-Chem produces higher ultimate yields of CHOCHO under low-NO_x conditions mainly due to DHDC formation and subsequent photolysis, neither of which are included in MCMv3.3.1. The NO_x-dependence of the CHOCHO yield in MCMv3.3.1 is similar to that of HCHO, implying that CHOCHO and HCHO observations would provide redundant information on isoprene emissions. The SENEX observations indicate that CHOCHO yields under low-NO_x conditions are too low in MCMv3.3.1, as discussed below. In GEOS-Chem, by contrast, the CHOCHO and HCHO yields show opposite dependences on NO_x, implying that they could provide complementary information on isoprene emissions.

3 Constraints from SENEX observations

Figure 3 shows the observed and simulated median vertical profiles of CHOCHO, HCHO, and NO_x concentrations along the SENEX flight tracks. Figure 4 shows maps of concentrations below 1 km altitude (above ground level) taken as the mixed layer. Here and elsewhere we only include daytime observations (10-17 local) and exclude targeted sampling of biomass burning plumes (diagnosed by acetonitrile concentrations above 200 pptv). CHOCHO, HCHO and NO_x were measured by the Airborne Cavity Enhanced Spectrometer (ACES) (Min et al., 2016), In-Situ Airborne Formaldehyde (ISAF) instrument (Cazorla et al., 2015), and the NOAA chemiluminescence instrument (Ryerson et al., 1999; Pollack et al., 2010), with stated accuracies of 6%, 10%, and 5% respectively.

Simulated median NO_x concentrations in the mixed layer are within 10% of observations, supporting the 50% reduction in EPA NEI NO_x emissions previously inferred from the analysis of SEAC^{4}RS observations by Travis et al. (2016), also included here (Section 2.1). Half of isoprene oxidation in the model under the SENEX conditions takes place by the low-NO_x pathways (Figure 1). Simulated median CHOCHO and HCHO concentrations in the mixed layer are within 20% of observations, but the model is too low at higher altitudes. During SENEX the mixed layer was typically capped by a neutrally stable transition layer of shallow cumulus convection which extended up to 3 km (Wagner et al., 2015), suggesting that transport via this mechanism

is underestimated in the model. Modeled CO concentrations are also negatively biased above the mixed layer (Figure S8), providing further support that convective transport in the model is underestimated.

The CHOCHO observations in the free troposphere (> 3 km) have to be treated with caution since they are below the reported instrument precision (32 pptv, Kaiser et al. (2015)). It is therefore difficult to determine whether the bias is due to a missing CHOCHO source in the model or instrument artifact. Elevated CHOCHO concentrations above the boundary layer have also been observed in previous campaigns over the Southeast US (Lee et al., 1998), California (Baidar et al., 2013), and the remote Pacific (Volkamer et al., 2015). There could be a free tropospheric source missing in the model, but it is unclear what this source could be, and correlative analysis of observed free tropospheric CHOCHO with other species measured in SENEX offer no insight ($r < 0.3$ for all observed VOCs).

The mixed layer concentrations maps in Figure 4 show that the model captures some of the horizontal variability in the observations. The spatial correlation for HCHO is high ($r = 0.75$) as in SEAC^{4}RS ($r = 0.64$, Zhu et al. (2016)), and reflects isoprene emission patterns. Correlation for CHOCHO is also relatively strong ($r = 0.51$). Temporally averaged CHOCHO and HCHO concentrations simulated by the model for the SENEX period (background in Figure 4) are much more uniform than those sampled along the SENEX flight tracks because of day-to-day variability in isoprene emissions, mostly driven by temperature (Zhu et al., 2016).

Figure 5 compares simulated and observed CHOCHO vs. HCHO relationships in the mixed layer color coded by $\mathrm{NO_x}$ concentrations. Correlation between the two species is strong. The model better captures the observed slope (0.028 modeled vs. 0.024 observed) compared to the AM3 CTM (0.045 and 0.035 with and without CHOCHO production from $\delta-\mathrm{ISOPO_2} + \mathrm{NO}$ respectively) (Li et al., 2016). Inclusion of aerosol uptake further reduces the bias to the observed slope (0.026, Figure S10). On average, CHOCHO is produced more promptly in AM3 compared to GEOS-Chem, which may lead to the higher slope. In the first few hours of oxidation this is due to a higher CHOCHO yield from $\mathrm{ISOPO_2}$ isomerization. Beyond the initial stages of isoprene oxidation, CHOCHO is produced faster in AM3 because of the increased fraction of CHOCHO produced from IEPOX over GLYC oxidation (Figure 1).

The strong correlation between CHOCHO and HCHO might suggest that they provide redundant information for constraining isoprene emissions. However, examination of Figure 5 indicates higher observed CHOCHO-to-HCHO ratios (R_{GF}) at low-$\mathrm{NO_x}$ concentrations, not captured by GEOS-Chem. Figure 6 shows the R_{GF} ratio as a function of $\mathrm{NO_x}$ below 1 km in the SENEX observations and as simulated by GEOS-Chem. Points are color coded by OH exposure time t_{OH} (Equation 1), derived from PTR-MS observations of the methylvinylketone + methacrolein-to-isoprene ratio (de Gouw and Warneke, 2007) following Wolfe et al. (2016). The median and interquartile R_{GF} values binned in 250 pptv $\mathrm{NO_x}$ increments are also shown. The observed median R_{GF} values (0.02 to 0.024 mol mol^{-1}) show no significant dependence on $\mathrm{NO_x}$, while GEOS-Chem shows a weak dependence. In both the model and observations there is a subset of low-$\mathrm{NO_x}$ points with higher R_{GF} values (0.03-0.06). These correspond to short OH exposure times and are caused by OH titration by isoprene. The high R_{GF} reflects the relatively faster production of CHOCHO than HCHO in the early stage of isoprene oxidation under low-$\mathrm{NO_x}$ conditions as shown by Figure 2. The presence of that population in the observations provides support for fast glyoxal production from the isomerization pathway of isoprene oxidation (Figure 1) that is present in GEOS-Chem but not in MCMv3.3.1.

Figure 6 also shows that there are is a small subset of points in GEOS-Chem with RGF values less than 0.01, reflecting low CHOCHO values in the model that are not found in the observations where the concentration floor is 0.05 ppbv (Figure 5). There may be a CHOCHO background missing from the model, possibly contributed by monoterpenes; MCMv3.3.1 predicts that the total CHOCHO yield from common monterpenes is high (Kaiser et al., 2015), and that they produce CHOCHO over a timescale of days (Figure S11).

4 Implications for satellite observations

Knowledge gained from SENEX enables an improved interpretation of CHOCHO and HCHO column observations from space in isoprene dominated environments. We use for this purpose June-August 2006-2007 observations of CHOCHO, HCHO, and tropospheric NO_2 columns from the Ozone Monitoring Instrument (OMI). OMI was launched onboard the NASA Aura satellite in July 2004, and provides daily global coverage in sun-synchronous orbit with an equatorial crossing time of 13:40 LT. The CHOCHO data are from the Smithsonian Astrophysical Observatory (SAO) retrieval described in Chan Miller et al. (2014) and hereby referred to as OMI SAO. The HCHO and NO_2 data are from the OMI Version 3 product release (González Abad et al., 2015; Bucsela et al., 2013). Retrievals are in the 435-461 nm spectral range for CHOCHO, 328.5-356.5 nm for HCHO, and 405-465 nm for NO_2. We use 2006-2007 data because 2013 data for CHOCHO are very noisy (Figure S12), possibly because of sensor degradation. The OMI observations are compared to a GEOS-Chem simulation covering the same period, at $2^\circ \times 2.5^\circ$ horizontal resolution.

Slant columns along the optical path of the backscattered solar radiation are fitted to the observed spectra and converted to vertical columns by division with an air mass factor (AMF) that accounts for the viewing geometry, atmospheric scattering, and the vertical profile of the gas (Palmer et al., 2001):

$$AMF = \int_0^\infty w(z)s(z)dz \tag{2}$$

Here $w(z)$ is the scattering weight measuring the sensitivity of the retrieval to the gas concentration at altitude z, and $s(z)$ is a normalized vertical profile of gas number density. Here we recomputed the AMFs for the three retrievals using vertical profiles from GEOS-Chem, as it is necessary for comparing simulated and observed vertical columns (Duncan et al., 2014).

We remove observations impacted by the row anomaly (http://www.knmi.nl/omi/research/product/rowanomaly-background.php), and those with cloud fractions over 20%. Previous validation of the OMI HCHO retrievals with SEAC^{4}RS aircraft observations revealed a 43% uniform low bias (Zhu et al., 2016), corrected in the data shown here.

Figure 7 compares CHOCHO and HCHO vertical columns from GEOS-Chem and OMI, and Figure 8 shows spatial correlations over the eastern US. Excellent agreement is found for HCHO, providing an independent test of the correction to the OMI HCHO retrieval inferred from the SEAC^{4}RS data (Zhu et al., 2016). Since GEOS-Chem can also replicate the HCHO-CHOCHO correlation in the SENEX data, the simulated CHOCHO columns can be used to indirectly validate the OMI CHOCHO observations. CHOCHO from OMI is highly correlated with GEOS-Chem ($r = 0.81$), indicative of the isoprene source.

However OMI CHOCHO shows a higher continental background and a factor of 2 weaker enhancement over the Southeast US.

Zhu et al. (2016) suggested that errors in the assumed surface reflectivities affecting the AMFs were an important source of the bias in the OMI HCHO retrievals. CHOCHO retrievals are even more sensitive to surface reflectivity because of the longer wavelengths. Russell et al. (2011) previously pointed out that the OMI surface reflectivities used in the standard NO_2 retrievals (Kleipool et al., 2008) were too high and replaced them with high resolution ($0.05° \times 0.05°$) reflectivity observations from MODIS (Schaaf and Wang, 2015) to produce the Berkeley High-Resolution (BEHR) OMI NO_2 retrieval. CHOCHO and NO_2 are retrieved at similar wavelengths so the sensitivity to surface reflectivity should be similar. Figure 7 (bottom right) shows the mean CHOCHO scattering weights computed from the OMI-SAO and BEHR. The lower BEHR surface reflectivity values result in a lower AMF and hence a higher vertical column (Figure 7, bottom left panel). The slope of the regression between GEOS-Chem and OMI CHOCHO columns increases from 0.48 to 0.62, improving but not reconciling the differences.

As pointed out above, SENEX and other observations suggest that GEOS-Chem may be missing a background source of CHOCHO. Integration of the median CHOCHO profile above 2 km in Figure 3 shows a negative model bias of 1.3×10^{14} molecules cm^{-2}, comparable to the continental background intercept in Figure 8 (1.9×10^{14} molecules cm^{-2}). The nonzero intercept may in part reflect an underestimate of CHOCHO concentrations caused by a missing CHOCHO source over the Southeast US, such as monoterpenes (Section 3). The presence of free tropospheric CHOCHO would further impact the AMF calculation under continental background conditions since the retrieval sensitivity as measured by the scattering weights increases with altitude. Thus the retrieved continental background would be overestimated.

Figure 9 shows CHOCHO vs. HCHO relationships for OMI (using the BEHR scattering weights) and GEOS-Chem, color coded by tropospheric NO_2 columns. Individual points are seasonal averages (data points from Figure 7) in order to limit noise. The slope is steeper in GEOS-Chem because the CHOCHO columns are higher. Since GEOS-Chem reproduces the aircraft CHOCHO-HCHO relationship without bias (Figure 5), this is further evidence of bias in the OMI CHOCHO observations. The CHOCHO-HCHO relationship is tight in both OMI ($r = 0.86$) and GEOS-Chem ($r = 0.99$), with no indication of a separate population of low-NO_x points with high R_{GF} as there was in the SENEX data. It thus appears from the OMI data that satellite observations of CHOCHO and HCHO in isoprene-dominated environments are redundant. This may reflect the higher NO_x levels in 2006-2007 compared to 2013 (Russell et al., 2012). However since median R_{GF} shows no significant variation with NO_x in the SENEX data (Figure 6), the required temporal averaging of satellite observations is a more likely explanation for the tight correlation. Finer-scale and more temporally resolved data, as will be available from the TEMPO geostationary instrument to be launched in the 2018-2020 time frame (Zoogman et al., 2016), may provide new perspectives of the utility of the CHOCHO retrieval.

5 Conclusions

We have used aircraft observations of glyoxal (CHOCHO), formaldehyde (HCHO), and related species from the SENEX aircraft campaign over the Southeast US together with OMI satellite data to better understand the CHOCHO yield from isoprene

and the complementarity of CHOCHO and HCHO observations from space for constraining isoprene emissions. This work includes a first validation of the CHOCHO retrieval from the OMI satellite instrument.

We began with an analysis of the time- and NO_x-dependent CHOCHO and HCHO yields from isoprene oxidation in the GEOS-Chem chemical transport model and in the Master Chemical Mechanism (MCMv3.3.1). The GEOS-Chem mechanism features several updates relevant to CHOCHO formation. These include a decrease in the $\delta-ISOPO_2 + NO$ branching ratio leading to prompt CHOCHO production under high-NO_x conditions, and a proposed low-NO_x pathway for prompt CHOCHO formation by photolysis of a di-hydroperoxide dicarbonyl compound (DHDC) product from (1,5)H-shift isomerization of dihydroperoxy α-formyl peroxy radicals in the $ISOPO_2$ isomerization pathway (Figure 1). GEOS-Chem and MCMv3.3.1 show similar HCHO yields from isoprene, increasing with increasing NO_x. CHOCHO yields from isoprene in MCMv3.3.1 show behavior similar to HCHO but GEOS-Chem has a higher yield at low-NO_x from the $ISOPO_2$ isomerization pathway.

Comparison of GEOS-Chem to the SENEX observations of CHOCHO and HCHO shows good agreement in the boundary layer but a negative CHOCHO model bias in the free troposphere. This could reflect an instrument artifact but may also imply a missing background source in the model. Mixed layer (< 1 km) observations show a strong CHOCHO-HCHO relationship that is reproduced in GEOS-Chem and is remarkably consistent across all conditions except at very low NO_x where the $[CHOCHO]/[HCHO]$ ratio (R_{GF}) can be unusually high. This reflects prompt formation of CHOCHO under low-NO_x conditions, which was missing from MCMv3.3.1 and is now simulated in our updated GEOS-Chem mechanism by DHDC photolysis.

The SENEX observations enable indirect validation of the OMI CHOCHO satellite data using GEOS-Chem as an intercomparison platform. The OMI data show a continental background that is consistent with the SENEX free tropospheric observations, and an enhancement over the Southeast US that is consistent with the isoprene source. However this enhancement is a factor of 2 too low in the OMI data. A partial explanation is that surface reflectivities assumed in the standard OMI retrieval are too high. The satellite data show strong CHOCHO-HCHO correlation consistent with the model and imply that the two gases provide redundant information for constraining isoprene emissions in regions where isoprene is their dominant precursor. This redundancy may reflect the seasonal averaging in the OMI data required to reduce noise. The HCHO satellite data are better validated (Zhu et al., 2016) and should therefore be preferentially used as proxy for isoprene emission. Future geostationary observations from TEMPO (Zoogman et al., 2016) will require less temporal averaging and this may reveal the utility of CHOCHO observations for estimating isoprene emissions under low-NO_x conditions when isoprene oxidation is titrated.

Acknowledgements. This work was funded by NASA ACMAP and ACCDAM and is a contribution to the NASA Aura Science Team. This research was undertaken with the assistance of resources provided at the NCI National Facility systems at the Australian National University through the National Computational Merit Allocation Scheme supported by the Australian Government. J.K., F.N.K., G.M.W., and T.F.H. acknowledge support from the US EPA Science to Achieve Results (STAR) program (grant 83540601).

References

Abbot, D. S., Palmer, P. I., Martin, R. V., Chance, K. V., Jacob, D. J., and Guenther, A.: Seasonal and interannual variability of North American isoprene emissions as determined by formaldehyde column measurements from space, Geophysical Research Letters, 30, n/a–n/a, 2003.

Alvarado, L. M. A., Richter, A., Vrekoussis, M., Wittrock, F., Hilboll, A., Schreier, S. F., and Burrows, J. P.: An improved glyoxal retrieval from OMI measurements, Atmospheric Measurement Techniques Discussions, 7, 5559–5599, doi:10.5194/amtd-7-5559-2014, http://www.atmos-meas-tech-discuss.net/7/5559/2014/, 2014.

Baidar, S., Oetjen, H., Coburn, S., Dix, B., Ortega, I., Sinreich, R., and Volkamer, R.: The CU Airborne MAX-DOAS instrument: vertical profiling of aerosol extinction and trace gases, Atmospheric Measurement Techniques, 6, 719–739, doi:10.5194/amt-6-719-2013, http://www.atmos-meas-tech.net/6/719/2013/, 2013.

Barkley, M. P., De Smedt, I., Van Roozendael, M., Kurosu, T. P., Chance, K., Arneth, A., Hagberg, D., Guenther, A., Paulot, F., Marais, E., and Mao, J.: Top-down isoprene emissions over tropical South America inferred from SCIAMACHY and OMI formaldehyde columns, Journal of Geophysical Research: Atmospheres, 118, 6849–6868, doi:10.1002/jgrd.50552, http://dx.doi.org/10.1002/jgrd.50552, 2013.

Bates, K. H., Crounse, J. D., Clair, J. M. S., Bennett, N. B., Nguyen, T. B., Seinfeld, J. H., Stoltz, B. M., and Wennberg, P. O.: Gas Phase Production and Loss of Isoprene Epoxydiols, The Journal of Physical Chemistry A, 118, 1237–1246, doi:10.1021/jp4107958, http://dx.doi.org/10.1021/jp4107958, pMID: 24476509, 2014.

Browne, E. C. and Cohen, R. C.: Effects of biogenic nitrate chemistry on the NO_x lifetime in remote continental regions, Atmospheric Chemistry and Physics, 12, 11 917–11 932, doi:10.5194/acp-12-11917-2012, http://www.atmos-chem-phys.net/12/11917/2012/, 2012.

Bucsela, E. J., Krotkov, N. A., Celarier, E. A., Lamsal, L. N., Swartz, W. H., Bhartia, P. K., Boersma, K. F., Veefkind, J. P., Gleason, J. F., and Pickering, K. E.: A new stratospheric and tropospheric NO_2 retrieval algorithm for nadir-viewing satellite instruments: applications to OMI, Atmospheric Measurement Techniques, 6, 2607–2626, doi:10.5194/amt-6-2607-2013, http://www.atmos-meas-tech.net/6/2607/2013/, 2013.

Carlton, A. G., Wiedinmyer, C., and Kroll, J. H.: A review of Secondary Organic Aerosol (SOA) formation from isoprene, Atmospheric Chemistry and Physics, 9, 4987–5005, doi:10.5194/acp-9-4987-2009, http://www.atmos-chem-phys.net/9/4987/2009/, 2009.

Cazorla, M., Wolfe, G. M., Bailey, S. A., Swanson, A. K., Arkinson, H. L., and Hanisco, T. F.: A new airborne laser-induced fluorescence instrument for in situ detection of formaldehyde throughout the troposphere and lower stratosphere, Atmospheric Measurement Techniques, 8, 541–552, doi:10.5194/amt-8-541-2015, http://www.atmos-meas-tech.net/8/541/2015/, 2015.

Chan Miller, C., Gonzalez Abad, G., Wang, H., Liu, X., Kurosu, T., Jacob, D. J., and Chance, K.: Glyoxal retrieval from the Ozone Monitoring Instrument, Atmospheric Measurement Techniques, 7, 3891–3907, doi:10.5194/amt-7-3891-2014, http://www.atmos-meas-tech.net/7/3891/2014/, 2014.

Chan Miller, C., Jacob, D. J., González Abad, G., and Chance, K.: Hotspot of glyoxal over the Pearl River delta seen from the OMI satellite instrument: implications for emissions of aromatic hydrocarbons, Atmospheric Chemistry and Physics, 16, 4631–4639, doi:10.5194/acp-16-4631-2016, http://www.atmos-chem-phys.net/16/4631/2016/, 2016.

Chance, K., Palmer, P. I., Spurr, R. J. D., Martin, R. V., Kurosu, T. P., and Jacob, D. J.: Satellite observations of formaldehyde over North America from GOME, Geophysical Research Letters, 27, 3461–3464, doi:10.1029/2000GL011857, http://dx.doi.org/10.1029/2000GL011857, 2000.

Crounse, J. D., Paulot, F., Kjaergaard, H. G., and Wennberg, P. O.: Peroxy radical isomerization in the oxidation of isoprene, Phys. Chem. Chem. Phys., 13, 13 607–13 613, doi:10.1039/C1CP21330J, http://dx.doi.org/10.1039/C1CP21330J, 2011.

Crounse, J. D., Nielsen, L. B., Jørgensen, S., Kjaergaard, H. G., and Wennberg, P. O.: Autoxidation of Organic Compounds in the Atmosphere, The Journal of Physical Chemistry Letters, 4, 3513–3520, doi:10.1021/jz4019207, http://dx.doi.org/10.1021/jz4019207, 2013.

Curci, G., Palmer, P. I., Kurosu, T. P., Chance, K., and Visconti, G.: Estimating European volatile organic compound emissions using satellite observations of formaldehyde from the Ozone Monitoring Instrument, Atmospheric Chemistry and Physics, 10, 11 501–11 517, doi:10.5194/acp-10-11501-2010, http://www.atmos-chem-phys.net/10/11501/2010/, 2010.

de Gouw, J. and Warneke, C.: Measurements of volatile organic compounds in the earth's atmosphere using proton-transfer-reaction mass spectrometry, Mass Spectrometry Reviews, 26, 223–257, doi:10.1002/mas.20119, http://dx.doi.org/10.1002/mas.20119, 2007.

DiGangi, J. P., Henry, S. B., Kammrath, A., Boyle, E. S., Kaser, L., Schnitzhofer, R., Graus, M., Turnipseed, A., Park, J.-H., Weber, R. J., Hornbrook, R. S., Cantrell, C. A., Maudlin III, R. L., Kim, S., Nakashima, Y., Wolfe, G. M., Kajii, Y., Apel, E., Goldstein, A. H., Guenther, A., Karl, T., Hansel, A., and Keutsch, F. N.: Observations of glyoxal and formaldehyde as metrics for the anthropogenic impact on rural photochemistry, Atmospheric Chemistry and Physics, 12, 9529–9543, doi:10.5194/acp-12-9529-2012, http://www.atmos-chem-phys.net/12/9529/2012/, 2012.

Duncan, B. N., Prados, A. I., Lamsal, L. N., Liu, Y., Streets, D. G., Gupta, P., Hilsenrath, E., Kahn, R. A., Nielsen, J. E., Beyersdorf, A. J., Burton, S. P., Fiore, A. M., Fishman, J., Henze, D. K., Hostetler, C. A., Krotkov, N. A., Lee, P., Lin, M., Pawson, S., Pfister, G., Pickering, K. E., Pierce, R. B., Yoshida, Y., and Ziemba, L. D.: Satellite data of atmospheric pollution for U.S. air quality applications: Examples of applications, summary of data end-user resources, answers to FAQs, and common mistakes to avoid, Atmospheric Environment, 94, 647 – 662, doi:http://dx.doi.org/10.1016/j.atmosenv.2014.05.061, http://www.sciencedirect.com/science/article/pii/S1352231014004270, 2014.

Emmerson, K. M. and Evans, M. J.: Comparison of tropospheric gas-phase chemistry schemes for use within global models, Atmospheric Chemistry and Physics, 9, 1831–1845, doi:10.5194/acp-9-1831-2009, http://www.atmos-chem-phys.net/9/1831/2009/, 2009.

Fisher, J. A., Jacob, D. J., Travis, K. R., Kim, P. S., Marais, E. A., Chan Miller, C., Yu, K., Zhu, L., Yantosca, R. M., Sulprizio, M. P., Mao, J., Wennberg, P. O., Crounse, J. D., Teng, A. P., Nguyen, T. B., St. Clair, J. M., Cohen, R. C., Romer, P., Nault, B. A., Wooldridge, P. J., Jimenez, J. L., Campuzano-Jost, P., Day, D. A., Shepson, P. B., Xiong, F., Blake, D. R., Goldstein, A. H., Misztal, P. K., Hanisco, T. F., Wolfe, G. M., Ryerson, T. B., Wisthaler, A., and Mikoviny, T.: Organic nitrate chemistry and its implications for nitrogen budgets in an isoprene- and monoterpene-rich atmosphere: constraints from aircraft (SEAC4RS) and ground-based (SOAS) observations in the Southeast US, Atmospheric Chemistry and Physics Discussions, 2016, 1–38, doi:10.5194/acp-2016-52, http://www.atmos-chem-phys-discuss.net/acp-2016-52/, 2016.

Fortems-Cheiney, A., Chevallier, F., Pison, I., Bousquet, P., Saunois, M., Szopa, S., Cressot, C., Kurosu, T. P., Chance, K., and Fried, A.: The formaldehyde budget as seen by a global-scale multi-constraint and multi-species inversion system, Atmospheric Chemistry and Physics, 12, 6699–6721, doi:10.5194/acp-12-6699-2012, http://www.atmos-chem-phys.net/12/6699/2012/, 2012.

Fu, T.-M., Jacob, D. J., Palmer, P. I., Chance, K., Wang, Y. X., Barletta, B., Blake, D. R., Stanton, J. C., and Pilling, M. J.: Space-based formaldehyde measurements as constraints on volatile organic compound emissions in east and south Asia and implications for ozone, J. Geophys. Res., 112, 2007.

Fu, T.-M., Jacob, D. J., Wittrock, F., Burrows, J. P., Vrekoussis, M., and Henze, D. K.: Global budgets of atmospheric glyoxal and methylglyoxal, and implications for formation of secondary organic aerosols, J. Geophys. Res., 113, http://dx.doi.org/10.1029/2007JD009505, 2008.

Galloway, M. M., Huisman, A. J., Yee, L. D., Chan, A. W. H., Loza, C. L., Seinfeld, J. H., and Keutsch, F. N.: Yields of oxidized volatile organic compounds during the OH radical initiated oxidation of isoprene, methyl vinyl ketone, and methacrolein under high-NO_x con-

ditions, Atmospheric Chemistry and Physics, 11, 10 779–10 790, doi:10.5194/acp-11-10779-2011, http://www.atmos-chem-phys.net/11/10779/2011/, 2011.

Geng, F., Tie, X., Guenther, A., Li, G., Cao, J., and Harley, P.: Effect of isoprene emissions from major forests on ozone formation in the city of Shanghai, China, Atmospheric Chemistry and Physics, 11, 10 449–10 459, doi:10.5194/acp-11-10449-2011, http://www.atmos-chem-phys.net/11/10449/2011/, 2011.

González Abad, G., Liu, X., Chance, K., Wang, H., Kurosu, T. P., and Suleiman, R.: Updated Smithsonian Astrophysical Observatory Ozone Monitoring Instrument (SAO OMI) formaldehyde retrieval, Atmospheric Measurement Techniques, 8, 19–32, doi:10.5194/amt-8-19-2015, http://www.atmos-meas-tech.net/8/19/2015/, 2015.

Guenther, A. B., Jiang, X., Heald, C. L., Sakulyanontvittaya, T., Duhl, T., Emmons, L. K., and Wang, X.: The Model of Emissions of Gases and Aerosols from Nature version 2.1 (MEGAN2.1): an extended and updated framework for modeling biogenic emissions, Geoscientific Model Development, 5, 1471–1492, doi:10.5194/gmd-5-1471-2012, http://www.geosci-model-dev.net/5/1471/2012/, 2012.

Jacob, D. J.: Heterogeneous chemistry and tropospheric ozone, Atmospheric Environment, 34, 2131 – 2159, doi:http://dx.doi.org/10.1016/S1352-2310(99)00462-8, http://www.sciencedirect.com/science/article/pii/S1352231099004628, 2000.

Jenkin, M. E., Young, J. C., and Rickard, A. R.: The MCM v3.3.1 degradation scheme for isoprene, Atmospheric Chemistry and Physics, 15, 11 433–11 459, doi:10.5194/acp-15-11433-2015, http://www.atmos-chem-phys.net/15/11433/2015/, 2015.

Kaiser, J., Wolfe, G. M., Min, K. E., Brown, S. S., Miller, C. C., Jacob, D. J., deGouw, J. A., Graus, M., Hanisco, T. F., Holloway, J., Peischl, J., Pollack, I. B., Ryerson, T. B., Warneke, C., Washenfelder, R. A., and Keutsch, F. N.: Reassessing the ratio of glyoxal to formaldehyde as an indicator of hydrocarbon precursor speciation, Atmospheric Chemistry and Physics, 15, 7571–7583, doi:10.5194/acp-15-7571-2015, http://www.atmos-chem-phys.net/15/7571/2015/, 2015.

Kim, P. S., Jacob, D. J., Fisher, J. A., Travis, K., Yu, K., Zhu, L., Yantosca, R. M., Sulprizio, M. P., Jimenez, J. L., Campuzano-Jost, P., Froyd, K. D., Liao, J., Hair, J. W., Fenn, M. A., Butler, C. F., Wagner, N. L., Gordon, T. D., Welti, A., Wennberg, P. O., Crounse, J. D., St. Clair, J. M., Teng, A. P., Millet, D. B., Schwarz, J. P., Markovic, M. Z., and Perring, A. E.: Sources, seasonality, and trends of southeast US aerosol: an integrated analysis of surface, aircraft, and satellite observations with the GEOS-Chem chemical transport model, Atmospheric Chemistry and Physics, 15, 10 411–10 433, doi:10.5194/acp-15-10411-2015, http://www.atmos-chem-phys.net/15/10411/2015/, 2015.

Kleipool, Q. L., Dobber, M. R., de Haan, J. F., and Levelt, P. F.: Earth surface reflectance climatology from 3 years of OMI data, Journal of Geophysical Research: Atmospheres, 113, n/a–n/a, 2008.

Laughner, J. L., Zare, A., and Cohen, R. C.: Effects of daily meteorology on the interpretation of space-based remote sensing of NO_2, Atmospheric Chemistry and Physics Discussions, 2016, 1–27, doi:10.5194/acp-2016-536, http://www.atmos-chem-phys-discuss.net/acp-2016-536/, 2016.

Lee, Y.-N., Zhou, X., Kleinman, L. I., Nunnermacker, L. J., Springston, S. R., Daum, P. H., Newman, L., Keigley, W. G., Holdren, M. W., Spicer, C. W., Young, V., Fu, B., Parrish, D. D., Holloway, J., Williams, J., Roberts, J. M., Ryerson, T. B., and Fehsenfeld, F. C.: Atmospheric chemistry and distribution of formaldehyde and several multioxygenated carbonyl compounds during the 1995 Nashville/Middle Tennessee Ozone Study, Journal of Geophysical Research: Atmospheres, 103, 22 449–22 462, doi:10.1029/98JD01251, http://dx.doi.org/10.1029/98JD01251, 1998.

Lerner, B. M., Gilman, J. B., Kuster, W. C., and de Gouw, J. A.: An improved, automated whole-air sampler and VOC GC-MS analysis system, (In preparation), 2016.

Li, J., Mao, J., Min, K.-E., Washenfelder, R. A., Brown, S. S., Kaiser, J., Keutsch, F. N., Volkamer, R., Wolfe, G. M., Hanisco, T. F., Pollack, I. B., Ryerson, T. B., Graus, M., Gilman, J. B., Lerner, B. M., Warneke, C., de Gouw, J. A., Middlebrook, A. M., Liao, J., Welti, A.,

Henderson, B. H., McNeill, V. F., Hall, S. R., Ullmann, K., Donner, L. J., Paulot, F., and Horowitz, L. W.: Observational constraints on glyoxal production from isoprene oxidation and its contribution to organic aerosol over the Southeast United States, Journal of Geophysical Research: Atmospheres, 121, 9849–9861, doi:10.1002/2016JD025331, http://dx.doi.org/10.1002/2016JD025331, 2016JD025331, 2016.

Madronich, S.: Photodissociation in the atmosphere: 1. Actinic flux and the effects of ground reflections and clouds, Journal of Geophysical Research: Atmospheres, 92, 9740–9752, doi:10.1029/JD092iD08p09740, http://dx.doi.org/10.1029/JD092iD08p09740, 1987.

Mao, J., Paulot, F., Jacob, D. J., Cohen, R. C., Crounse, J. D., Wennberg, P. O., Keller, C. A., Hudman, R. C., Barkley, M. P., and Horowitz, L. W.: Ozone and organic nitrates over the eastern United States: Sensitivity to isoprene chemistry, Journal of Geophysical Research: Atmospheres, 118, 11,256–11,268, doi:10.1002/jgrd.50817, http://dx.doi.org/10.1002/jgrd.50817, 2013.

Marais, E. A., Jacob, D. J., Kurosu, T. P., Chance, K., Murphy, J. G., Reeves, C., Mills, G., Casadio, S., Millet, D. B., Barkley, M. P., Paulot, F., and Mao, J.: Isoprene emissions in Africa inferred from OMI observations of formaldehyde columns, Atmospheric Chemistry and Physics, 12, 6219–6235, doi:10.5194/acp-12-6219-2012, http://www.atmos-chem-phys.net/12/6219/2012/, 2012.

Marais, E. A., Jacob, D. J., Jimenez, J. L., Campuzano-Jost, P., Day, D. A., Hu, W., Krechmer, J., Zhu, L., Kim, P. S., Miller, C. C., Fisher, J. A., Travis, K., Yu, K., Hanisco, T. F., Wolfe, G. M., Arkinson, H. L., Pye, H. O. T., Froyd, K. D., Liao, J., and McNeill, V. F.: Aqueous-phase mechanism for secondary organic aerosol formation from isoprene: application to the southeast United States and co-benefit of SO2 emission controls, Atmospheric Chemistry and Physics, 16, 1603–1618, doi:10.5194/acp-16-1603-2016, http://www.atmos-chem-phys.net/16/1603/2016/, 2016.

Millet, D. B., Jacob, D. J., Boersma, K. F., Fu, T.-M., Kurosu, T. P., Chance, K., Heald, C. L., and Guenther, A.: Spatial distribution of isoprene emissions from North America derived from formaldehyde column measurements by the OMI satellite sensor, Journal of Geophysical Research: Atmospheres, 113, n/a–n/a, http://dx.doi.org/10.1029/2007JD008950, 2008.

Min, K.-E., Washenfelder, R. A., Dubé, W. P., Langford, A. O., Edwards, P. M., Zarzana, K. J., Stutz, J., Lu, K., Rohrer, F., Zhang, Y., and Brown, S. S.: A broadband cavity enhanced absorption spectrometer for aircraft measurements of glyoxal, methylglyoxal, nitrous acid, nitrogen dioxide, and water vapor, Atmospheric Measurement Techniques, 9, 423–440, doi:10.5194/amt-9-423-2016, http://www.atmos-meas-tech.net/9/423/2016/, 2016.

Molod, A., Takacs, L., Suarez, M., Bacmeister, J., Song, I.-S., and Eichmann, A.: The GEOS-5 Atmospheric General Circulation Model: Mean Climate and Development from MERRA to Fortuna, Tech. Rep. NASA/TM–2012-104606/Vol 28, Nasa Godard Space Flight Center, 2012.

Müller, J.-F., Peeters, J., and Stavrakou, T.: Fast photolysis of carbonyl nitrates from isoprene, Atmospheric Chemistry and Physics, 14, 2497–2508, doi:10.5194/acp-14-2497-2014, http://www.atmos-chem-phys.net/14/2497/2014/, 2014.

Palmer, P. I., Jacob, D. J., Chance, K., Martin, R. V., Spurr, R. J. D., Kurosu, T. P., Bey, I., Yantosca, R., Fiore, A., and Li, Q.: Air mass factor formulation for spectroscopic measurements from satellites: Application to formaldehyde retrievals from the Global Ozone Monitoring Experiment, Journal of Geophysical Research: Atmospheres, 106, 14 539–14 550, http://dx.doi.org/10.1029/2000JD900772, 2001.

Palmer, P. I., Jacob, D. J., Fiore, A. M., Martin, R. V., Chance, K., and Kurosu, T. P.: Mapping isoprene emissions over North America using formaldehyde column observations from space, Journal of Geophysical Research: Atmospheres, 108, n/a–n/a, doi:10.1029/2002JD002153, http://dx.doi.org/10.1029/2002JD002153, 2003.

Palmer, P. I., Abbot, D. S., Fu, T.-M., Jacob, D. J., Chance, K., Kurosu, T. P., Guenther, A., Wiedinmyer, C., Stanton, J. C., Pilling, M. J., Pressley, S. N., Lamb, B., and Sumner, A. L.: Quantifying the seasonal and interannual variability of North American isoprene emissions using satellite observations of the formaldehyde column, Journal of Geophysical Research: Atmospheres, 111, n/a–n/a, http://dx.doi.org/10.1029/2005JD006689, 2006.

Paulot, F., Crounse, J. D., Kjaergaard, H. G., Kroll, J. H., Seinfeld, J. H., and Wennberg, P. O.: Isoprene photooxidation: new insights into the production of acids and organic nitrates, Atmospheric Chemistry and Physics, 9, 1479–1501, doi:10.5194/acp-9-1479-2009, http://www.atmos-chem-phys.net/9/1479/2009/, 2009a.

Paulot, F., Crounse, J. D., Kjaergaard, H. G., Kürten, A., St. Clair, J. M., Seinfeld, J. H., and Wennberg, P. O.: Unexpected Epoxide Formation in the Gas-Phase Photooxidation of Isoprene, Science, 325, 730–733, doi:10.1126/science.1172910, http://www.sciencemag.org/content/325/5941/730.abstract, 2009b.

Peeters, J. and Muller, J.-F.: HOx radical regeneration in isoprene oxidation via peroxy radical isomerisations. II: experimental evidence and global impact, Phys. Chem. Chem. Phys., 12, 14 227–14 235, doi:10.1039/C0CP00811G, http://dx.doi.org/10.1039/C0CP00811G, 2010.

Peeters, J., Nguyen, T. L., and Vereecken, L.: HOx radical regeneration in the oxidation of isoprene, Phys. Chem. Chem. Phys., 11, 5935–5939, doi:10.1039/B908511D, http://dx.doi.org/10.1039/B908511D, 2009.

Peeters, J., Müller, J.-F., Stavrakou, T., and Nguyen, V. S.: Hydroxyl Radical Recycling in Isoprene Oxidation Driven by Hydrogen Bonding and Hydrogen Tunneling: The Upgraded LIM1 Mechanism, The Journal of Physical Chemistry A, 118, 8625–8643, doi:10.1021/jp5033146, http://dx.doi.org/10.1021/jp5033146, pMID: 25010574, 2014.

Pollack, I. B., Lerner, B. M., and Ryerson, T. B.: Evaluation of ultraviolet light-emitting diodes for detection of atmospheric NO2 by photolysis - chemiluminescence, Journal of Atmospheric Chemistry, 65, 111–125, doi:10.1007/s10874-011-9184-3, http://dx.doi.org/10.1007/s10874-011-9184-3, 2010.

Russell, A. R., Perring, A. E., Valin, L. C., Bucsela, E. J., Browne, E. C., Wooldridge, P. J., and Cohen, R. C.: A high spatial resolution retrieval of NO₂ column densities from OMI: method and evaluation, Atmospheric Chemistry and Physics, 11, 8543–8554, doi:10.5194/acp-11-8543-2011, http://www.atmos-chem-phys.net/11/8543/2011/, 2011.

Russell, A. R., Valin, L. C., and Cohen, R. C.: Trends in OMI NO_2 observations over the United States: effects of emission control technology and the economic recession, Atmospheric Chemistry and Physics, 12, 12 197–12 209, doi:10.5194/acp-12-12197-2012, http://www.atmos-chem-phys.net/12/12197/2012/, 2012.

Ryerson, T. B., Huey, L. G., Knapp, K., Neuman, J. A., Parrish, D. D., Sueper, D. T., and Fehsenfeld, F. C.: Design and initial characterization of an inlet for gas-phase NOy measurements from aircraft, Journal of Geophysical Research: Atmospheres, 104, 5483–5492, doi:10.1029/1998JD100087, http://dx.doi.org/10.1029/1998JD100087, 1999.

Schaaf, C. and Wang, Z.: MCD43C3 MODIS/Terra+Aqua BRDF/Albedo Albedo Daily L3 Global 0.05Deg CMG V006., Tech. Rep. doi:10.5067/MODIS/MCD43C3.006, NASA EOSDIS Land Processes DAAC, 2015.

Stavrakou, T., Peeters, J., and Müller, J.-F.: Improved global modelling of HO_x recycling in isoprene oxidation: evaluation against the GABRIEL and INTEX-A aircraft campaign measurements, Atmospheric Chemistry and Physics, 10, 9863–9878, doi:10.5194/acp-10-9863-2010, http://www.atmos-chem-phys.net/10/9863/2010/, 2010.

Toon, O. B., Maring, H., Dibb, J., Ferrare, R., Jacob, D. J., Jensen, E. J., Luo, Z. J., Mace, G. G., Pan, L. L., Pfister, L., Rosenlof, K. H., Redemann, J., Reid, J. S., Singh, H. B., Thompson, A. M., Yokelson, R., Minnis, P., Chen, G., Jucks, K. W., and Pszenny, A.: Planning, implementation, and scientific goals of the Studies of Emissions and Atmospheric Composition, Clouds and Climate Coupling by Regional Surveys (SEAC4RS) field mission, Journal of Geophysical Research: Atmospheres, 121, 4967–5009, doi:10.1002/2015JD024297, http://dx.doi.org/10.1002/2015JD024297, 2015JD024297, 2016.

Travis, K. R., Jacob, D. J., Fisher, J. A., Kim, P. S., Marais, E. A., Zhu, L., Yu, K., Miller, C. C., Yantosca, R. M., Sulprizio, M. P., Thompson, A. M., Wennberg, P. O., Crounse, J. D., St. Clair, J. M., Cohen, R. C., Laughner, J. L., Dibb, J. E., Hall, S. R., Ullmann, K., Wolfe, G. M., Pollack, I. B., Peischl, J., Neuman, J. A., and Zhou, X.: Why do models overestimate surface ozone in the Southeast United States?,

Atmospheric Chemistry and Physics, 16, 13 561–13 577, doi:10.5194/acp-16-13561-2016, http://www.atmos-chem-phys.net/16/13561/2016/, 2016.

Volkamer, R., Platt, U., and Wirtz, K.: Primary and Secondary Glyoxal Formation from Aromatics: Experimental Evidence for the Bicycloalkyl-Radical Pathway from Benzene, Toluene, and p-Xylene, The Journal of Physical Chemistry A, 105, 7865–7874, doi:10.1021/jp010152w, http://dx.doi.org/10.1021/jp010152w, 2001.

Volkamer, R., Baidar, S., Campos, T. L., Coburn, S., DiGangi, J. P., Dix, B., Eloranta, E. W., Koenig, T. K., Morley, B., Ortega, I., Pierce, B. R., Reeves, M., Sinreich, R., Wang, S., Zondlo, M. A., and Romashkin, P. A.: Aircraft measurements of BrO, IO, glyoxal, NO_2, H_2O, O_2–O_2 and aerosol extinction profiles in the tropics: comparison with aircraft-/ship-based in situ and lidar measurements, Atmospheric Measurement Techniques, 8, 2121–2148, doi:10.5194/amt-8-2121-2015, http://www.atmos-meas-tech.net/8/2121/2015/, 2015.

Vrekoussis, M., Wittrock, F., Richter, A., and Burrows, J. P.: Temporal and spatial variability of glyoxal as observed from space, Atmospheric Chemistry and Physics, 9, 4485–4504, doi:10.5194/acp-9-4485-2009, http://www.atmos-chem-phys.net/9/4485/2009/, 2009.

Vrekoussis, M., Wittrock, F., Richter, A., and Burrows, J. P.: GOME-2 observations of oxygenated VOCs: what can we learn from the ratio glyoxal to formaldehyde on a global scale?, Atmospheric Chemistry and Physics, 10, 10 145–10 160, doi:10.5194/acp-10-10145-2010, http://www.atmos-chem-phys.net/10/10145/2010/, 2010.

Wagner, N. L., Brock, C. A., Angevine, W. M., Beyersdorf, A., Campuzano-Jost, P., Day, D., de Gouw, J. A., Diskin, G. S., Gordon, T. D., Graus, M. G., Holloway, J. S., Huey, G., Jimenez, J. L., Lack, D. A., Liao, J., Liu, X., Markovic, M. Z., Middlebrook, A. M., Mikoviny, T., Peischl, J., Perring, A. E., Richardson, M. S., Ryerson, T. B., Schwarz, J. P., Warneke, C., Welti, A., Wisthaler, A., Ziemba, L. D., and Murphy, D. M.: In situ vertical profiles of aerosol extinction, mass, and composition over the southeast United States during SENEX and SEAC⁴RS: observations of a modest aerosol enhancement aloft, Atmospheric Chemistry and Physics, 15, 7085–7102, doi:10.5194/acp-15-7085-2015, http://www.atmos-chem-phys.net/15/7085/2015/, 2015.

Warneke, C., Trainer, M., de Gouw, J. A., Parrish, D. D., Fahey, D. W., Ravishankara, A. R., Middlebrook, A. M., Brock, C. A., Roberts, J. M., Brown, S. S., Neuman, J. A., Lerner, B. M., Lack, D., Law, D., Huebler, G., Pollack, I., Sjostedt, S., Ryerson, T. B., Gilman, J. B., Liao, J., Holloway, J., Peischl, J., Nowak, J. B., Aikin, K., Min, K.-E., Washenfelder, R. A., Graus, M. G., Richardson, M., Markovic, M. Z., Wagner, N. L., Welti, A., Veres, P. R., Edwards, P., Schwarz, J. P., Gordon, T., Dube, W. P., McKeen, S., Brioude, J., Ahmadov, R., Bougiatioti, A., Lin, J., Nenes, A., Wolfe, G. M., Hanisco, T. F., Lee, B. H., Lopez-Hilfiker, F. D., Thornton, J. A., Keutsch, F. N., Kaiser, J., Mao, J., and Hatch, C.: Instrumentation and Measurement Strategy for the NOAA SENEX Aircraft Campaign as Part of the Southeast Atmosphere Study 2013, Atmospheric Measurement Techniques Discussions, 2016, 1–39, doi:10.5194/amt-2015-388, http://www.atmos-meas-tech-discuss.net/amt-2015-388/, 2016.

Wittrock, F., Richter, A., Oetjen, H., Burrows, J. P., Kanakidou, M., Myriokefalitakis, S., Volkamer, R., Beirle, S., Platt, U., and Wagner, T.: Simultaneous global observations of glyoxal and formaldehyde from space, Geophysical Research Letters, 33, 2006.

Wolfe, G. M., Kaiser, J., Hanisco, T. F., Keutsch, F. N., de Gouw, J. A., Gilman, J. B., Graus, M., Hatch, C. D., Holloway, J., Horowitz, L. W., Lee, B. H., Lerner, B. M., Lopez-Hilifiker, F., Mao, J., Marvin, M. R., Peischl, J., Pollack, I. B., Roberts, J. M., Ryerson, T. B., Thornton, J. A., Veres, P. R., and Warneke, C.: Formaldehyde production from isoprene oxidation across NOx regimes, Atmospheric Chemistry and Physics, 16, 2597–2610, doi:10.5194/acp-16-2597-2016, http://www.atmos-chem-phys.net/16/2597/2016/, 2016.

Yu, K., Jacob, D. J., Fisher, J. A., Kim, P. S., Marais, E. A., Miller, C. C., Travis, K. R., Zhu, L., Yantosca, R. M., Sulprizio, M. P., Cohen, R. C., Dibb, J. E., Fried, A., Mikoviny, T., Ryerson, T. B., Wennberg, P. O., and Wisthaler, A.: Sensitivity to grid resolution in the ability of a chemical transport model to simulate observed oxidant chemistry under high-isoprene conditions, Atmospheric Chemistry and Physics Discussions, 2016, 1–16, doi:10.5194/acp-2015-980, http://www.atmos-chem-phys-discuss.net/acp-2015-980/, 2016.

Zhu, L., Jacob, D. J., Kim, P. S., Fisher, J. A., Yu, K., Travis, K. R., Mickley, L. J., Yantosca, R. M., Sulprizio, M. P., De Smedt, I., González Abad, G., Chance, K., Li, C., Ferrare, R., Fried, A., Hair, J. W., Hanisco, T. F., Richter, D., Jo Scarino, A., Walega, J., Weibring, P., and Wolfe, G. M.: Observing atmospheric formaldehyde (HCHO) from space: validation and intercomparison of six retrievals from four satellites (OMI, GOME2A, GOME2B, OMPS) with SEAC^{4}RS aircraft observations over the southeast US, Atmospheric Chemistry and Physics, 16, 13 477–13 490, doi:10.5194/acp-16-13477-2016, http://www.atmos-chem-phys.net/16/13477/2016/, 2016.

Zoogman, P., Liu, X., Suleiman, R., Pennington, W., Flittner, D., Al-Saadi, J., Hilton, B., Nicks, D., Newchurch, M., Carr, J., Janz, S., Andraschko, M., Arola, A., Baker, B., Canova, B., Miller, C. C., Cohen, R., Davis, J., Dussault, M., Edwards, D., Fishman, J., Ghulam, A., Abad, G. G., Grutter, M., Herman, J., Houck, J., Jacob, D., Joiner, J., Kerridge, B., Kim, J., Krotkov, N., Lamsal, L., Li, C., Lindfors, A., Martin, R., McElroy, C., McLinden, C., Natraj, V., Neil, D., Nowlan, C., O'Sullivan, E., Palmer, P., Pierce, R., Pippin, M., Saiz-Lopez, A., Spurr, R., Szykman, J., Torres, O., Veefkind, J., Veihelmann, B., Wang, H., Wang, J., and Chance, K.: Tropospheric emissions: Monitoring of pollution (TEMPO), Journal of Quantitative Spectroscopy and Radiative Transfer, pp. –, doi:http://dx.doi.org/10.1016/j.jqsrt.2016.05.008, http://www.sciencedirect.com/science/article/pii/S0022407316300863, 2016.

Figures

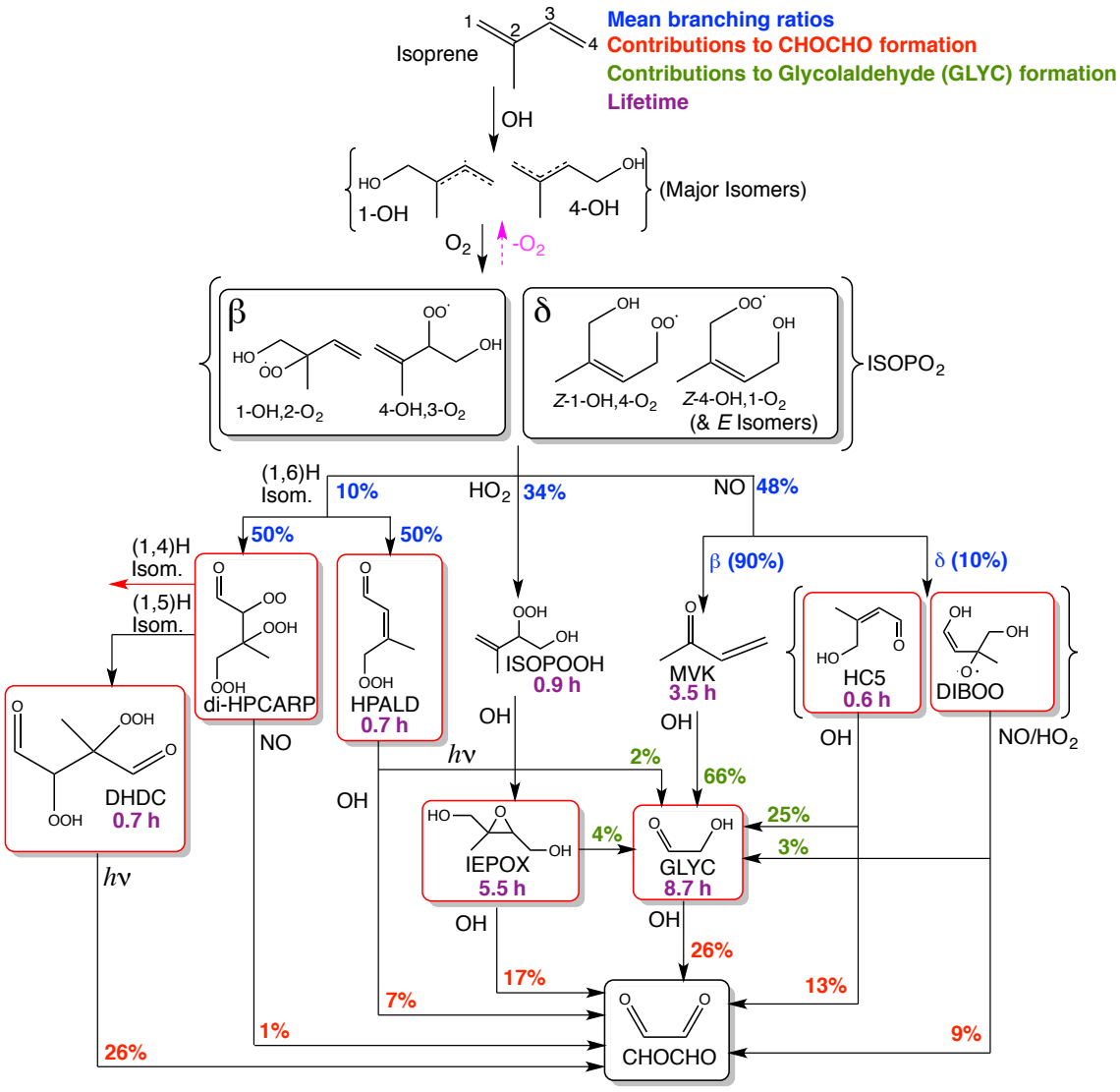

Figure 1. Pathways for glyoxal (CHOCHO) formation from isoprene oxidation in GEOS-Chem as implemented in this work. Only species relevant to CHOCHO formation are shown. Branching ratios, species lifetimes, and contributions to glyoxal and glycolaldehyde (GLYC) formation from each boxed species are mean values over the Southeast United States ($96.25 - 73.75°$W, $29 - 41°$N) during the SENEX campaign (June 1st - July 10th 2013). Species lifetimes are shown for an OH concentration of 4×10^6 molecules cm^{-3}.

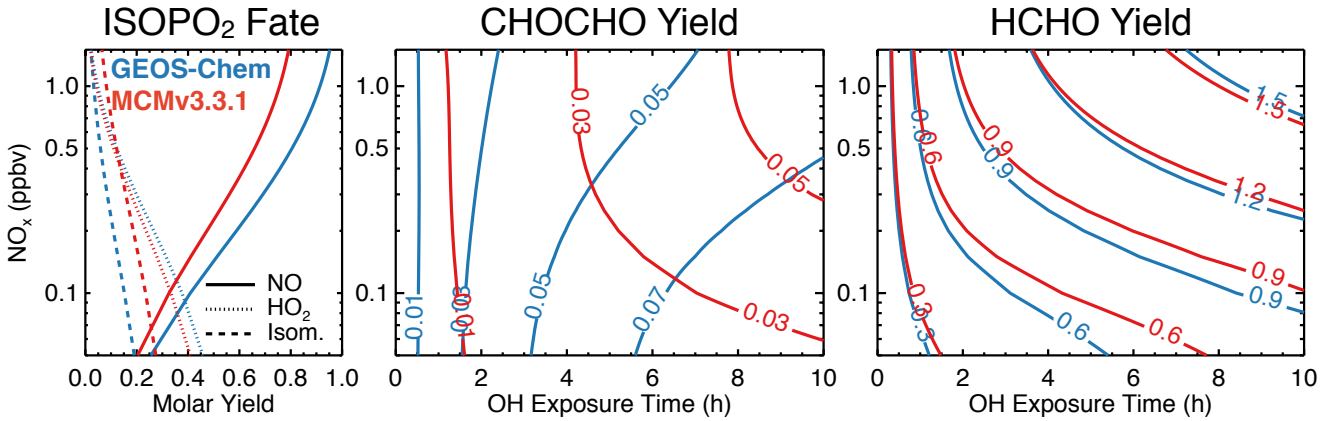

Figure 2. Cumulative time- and NO_x dependent molar yields of CHOCHO and HCHO from isoprene oxidation in the GEOS-Chem and MCM3.3.1 chemical mechanisms. Results are from box model simulations with fixed NO_x concentration as described in the text, and are presented as functions of the imposed NO_x concentration (vertical axis). The left panel shows the isoprene peroxy radical ($ISOPO_2$) branching ratios for reaction with NO, HO_2, and isomerization. The middle and right panels show the time-dependent cumulative yields of CHOCHO and HCHO, where time is normalized by OH exposure (Equation 1). "OH exposure time" is equivalent to time for a constant [OH] = 4×10^6 molecules cm^{-3}.

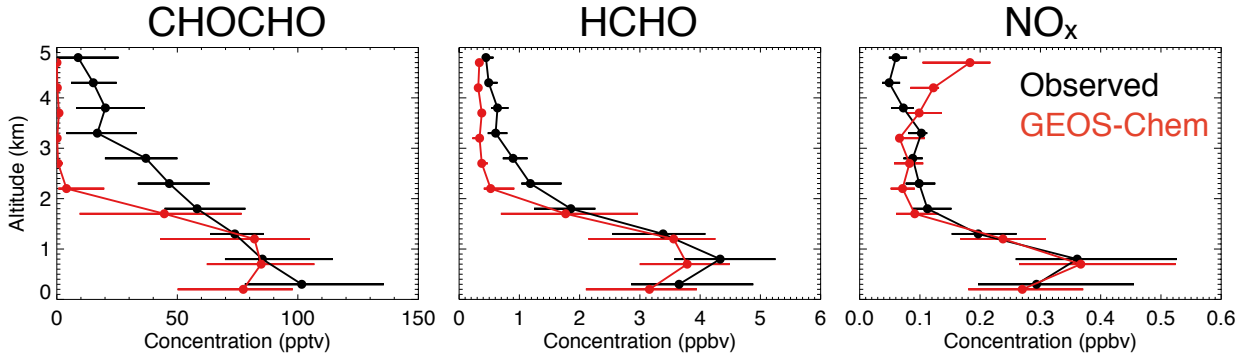

Figure 3. Median vertical profiles of CHOCHO, HCHO, and NO_x concentrations during SENEX (June 1 - July 10 2013). Observed concentrations (Min et al., 2016; Cazorla et al., 2015; Pollack et al., 2010) are compared to GEOS-Chem model values sampled along the flight tracks. Horizontal bars indicate interquartile range. Altitudes are above ground level (AGL).

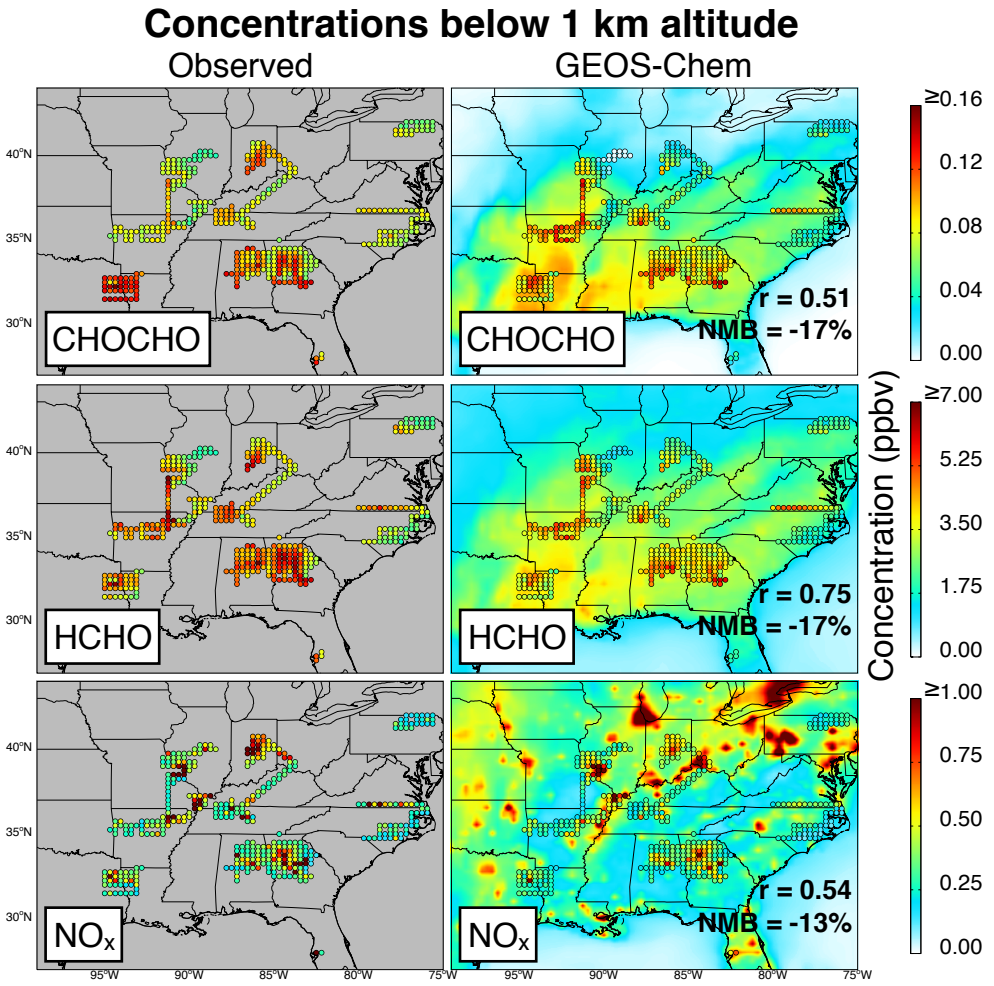

Figure 4. CHOCHO, HCHO, and NO_x concentrations below 1 km AGL during SENEX (June 1 - July 10 2013). The grid squares show daytime aircraft observations compared to the colocated GEOS-Chem model values on the $0.25^\circ \times 0.3125^\circ$ model grid. Background contours in the right panels show the average model-simulated concentrations at 13 - 14 local time for the SENEX period. Comparison statistics between model and observation grid squares are shown as the correlation coefficient r and the normalized mean bias (NMB). Correlation statistics for NO_2 exclude urban plumes in the observations ($[NO_x] > 4$ ppb) as these would not be resolved at the scale of the model.

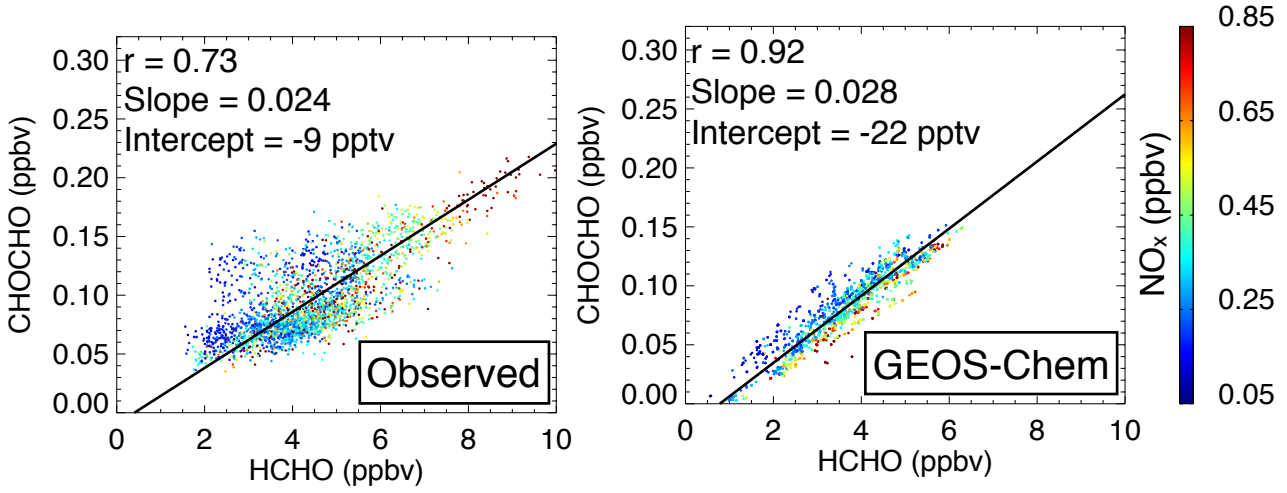

Figure 5. Relationship between CHOCHO and HCHO concentrations in the mixed layer (< 1 km AGL) during SENEX (June 1 - July 10 2013), color coded by NO_x concentration. Observed concentrations (Min et al., 2016; Cazorla et al., 2015) are compared to GEOS-Chem model values sampled along the flight tracks. Lines and reported slopes are from reduced major axis regressions.

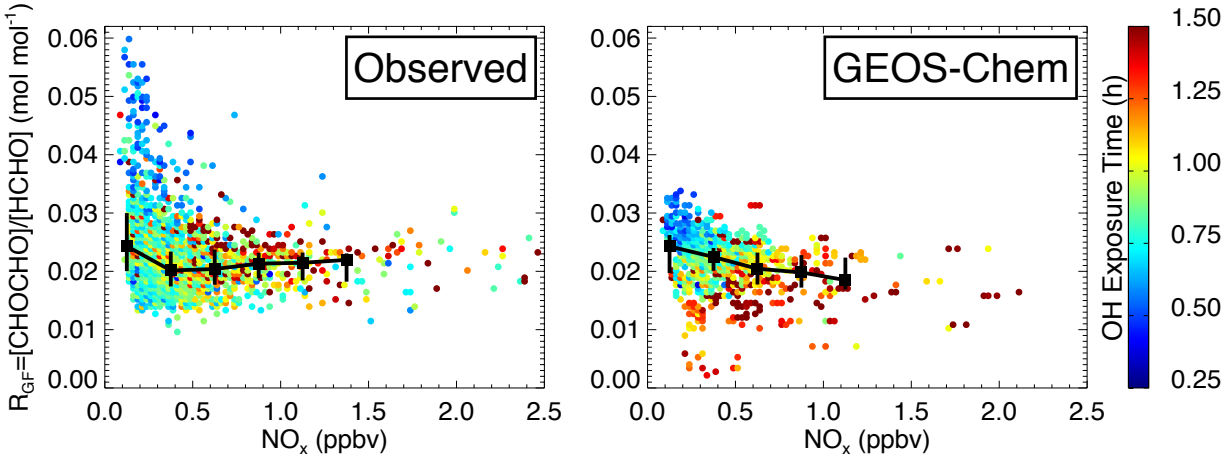

Figure 6. Dependence of the CHOCHO-to-HCHO ratio R_{GF} on NO_x concentrations for the SENEX conditions. Observations below 1 km altitude (left) are compared to GEOS-Chem model values sampled along the flight tracks (right). Points are color coded by the OH exposure time t_{OH} (Equation 1). Binned median and interquartile R_{GF} values in increments of 250 pptv NO_x for bins with more than 20 values are also shown.

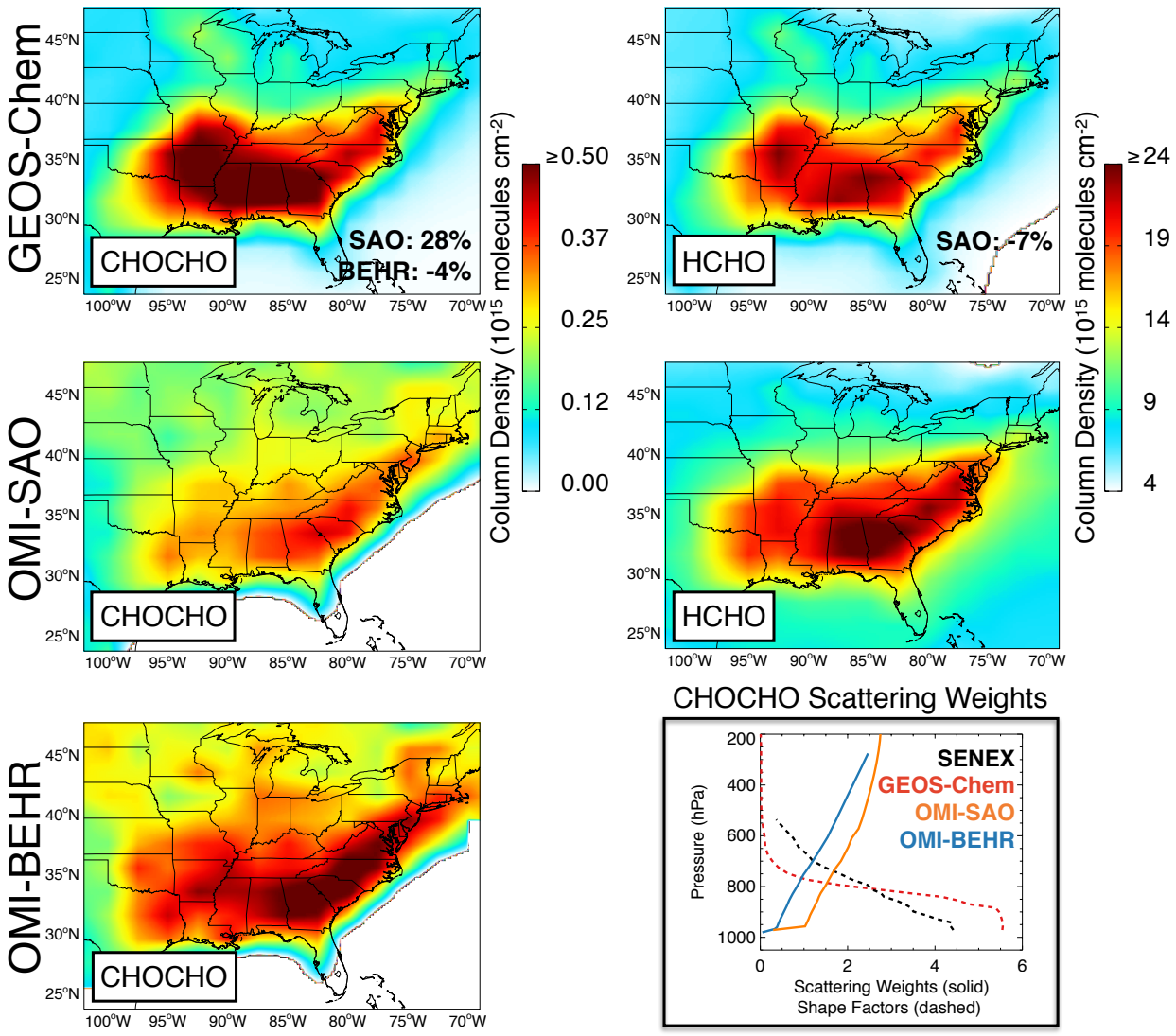

Figure 7. Mean CHOCHO and HCHO columns in summer (JJA) 2006-2007. GEOS-Chem model values (top) are compared to OMI satellite observations (middle and bottom). OMI-SAO is the standard operational product (Chan Miller et al., 2014; González Abad et al., 2015). The OMI-BEHR product for CHOCHO uses tropospheric scattering weights from the BEHR NO_2 retrieval (Russell et al., 2011; Laughner et al., 2016). The OMI HCHO observations have been scaled up by a factor of 1.67 to correct for retrieval bias (Zhu et al., 2016). The normalized mean bias (NMB) between GEOS-Chem and OMI in the Southeast US ($75^\circ - 100^\circ$W, $29.5^\circ - 37.5^\circ$N) is shown within the GEOS-Chem panels. The bottom right panel shows the mean CHOCHO scattering weights (w) from the OMI-SAO and OMI-BEHR retrievals and the vertical shape factors (s) over the Southeast US from the SENEX observations and GEOS-Chem in the Southeast US from a typical orbit (10114, 9 June 2006).

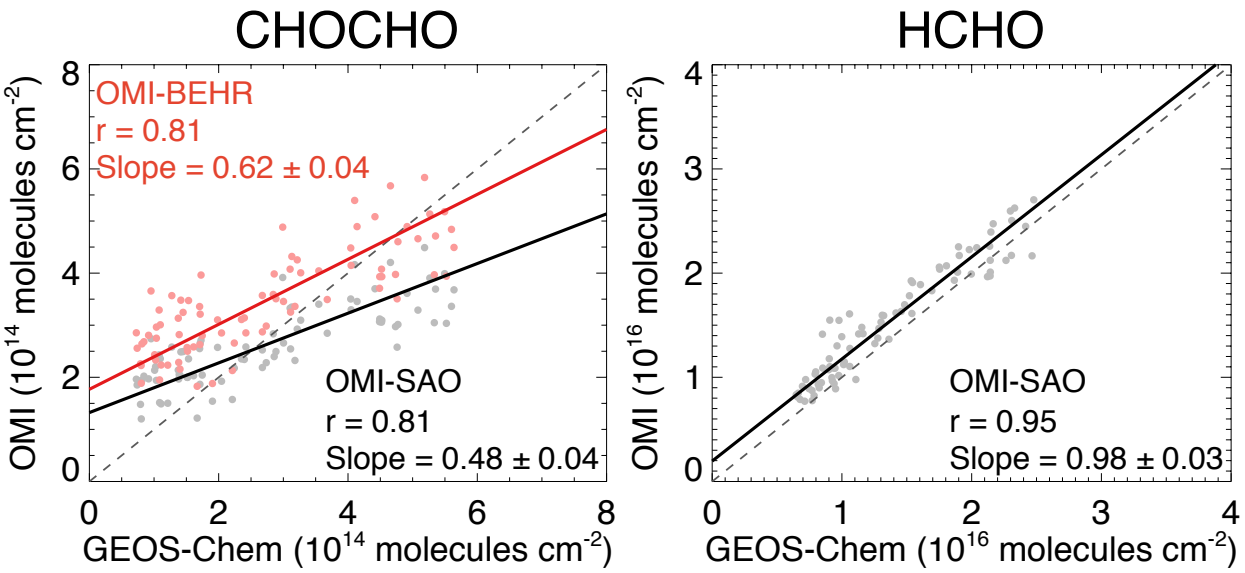

Figure 8. scatter plots of OMI vs. GEOS-Chem CHOCHO and HCHO columns over the eastern US ($75° - 100°$W, $29.5° - 45°$N). Values are seasonal means for JJA 2006-2007 as plotted in Figure 7. OMI observations for CHOCHO are from the standard SAO retrieval (Chan Miller et al., 2014) and using BEHR scattering weights (Russell et al., 2011; Laughner et al., 2016). Correlation coefficients and reduced-major-axis (RMA) regressions are shown.

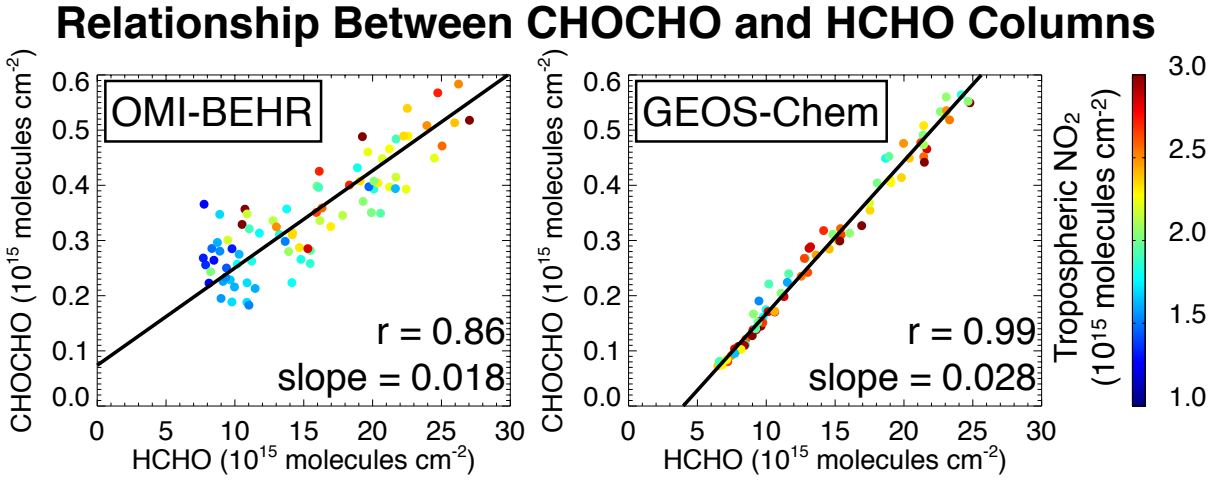

Figure 9. Relationship between CHOCHO and HCHO vertical columns over the eastern US ($75° - 100°$W, $29.5° - 45°$N) in June-August 2006-2007 color coded by tropospheric NO_2 columns. OMI values with CHOCHO AMFs computed from BEHR scattering weights are compared to GEOS-Chem values. Lines and reported slopes are from reduced major axis regressions.